Bond softening in monolayer graphite formed on transition-metal carbide surfaces

T. Aizawa, R. Souda, S. Otani, and Y. Ishizawa
National Institute for Research in Inorganic Materials, 1-1 Namiki, Tsukuba, Ibaraki 305, Japan

C. Oshima
Department of Applied Physics, Waseda University, 3-4-1 Okubo, Shinjuku-ku, Tokyo 169, Japan
(Received 23 February 1990; revised manuscript received 16 August 1990)

Full phonon-dispersion curves of the graphitic layer on some transition-metal carbides were measured by using high-resolution electron-energy-loss spectroscopy. The graphitic layer on (111) surfaces of TaC, HfC, and TiC showed anomalous softening within the layer, whereas the graphite layer on TaC(001) is similar to bulk graphite. The measured phonon dispersion has been analyzed with a force-constant model, and it has been revealed that the force constants for vertical angle bending and for bond twisting are much weaker in the former case. This is ascribed to the charge transfer into the overlayer from the substrate, resulting in the weakening of the π bond in graphite. The clear contrast in variations of phonons between the graphitic layer on TaC(111) and that on TaC(001) indicates that the microscopic structure at the interface determines the charge transfer.

I. INTRODUCTION

Graphite is one of the simplest layered materials and is widely used in new branches of modern science and technology. For example, in surface science, the inert surface characteristics related to graphite's specific electronic structure have been utilized in its use as a standard surface in scanning tunneling microscopy,[1,2] atomic-force microscopy,[3] and as a well-defined substrate in ultralow-temperature experiments of two-dimensional inert-gas solids.[4] Since a graphite layer completely bonds within itself and has no dangling bond, the interaction is thought to be very weak or van der Waals–like between the layer and its surroundings, which is the adjoining layer in bulk graphite, the substrate in the case of monolayer graphite, the adsorbate in an adsorption system that uses graphite as the substrate, and the intercalant in graphite intercalation compounds. This property is the cause of the remarkable behavior of graphite which includes intercalation,[5,6] lubrication, and so on, that has been of considerable practical interest in the research fields of material-science, vacuum, and nuclear-fusion technology.

Recently, graphitic carbon on transition-metal surfaces has attracted wide interest, and the presence of monolayer graphite has been established from low-energy-electron diffraction (LEED) and Auger-electron spectroscopy (AES) experiments.[7–15] In the case of graphite on Ni(111),[7–9] in which the overlayer makes an exceptionally commensurate epitaxial structure, it is well established that the stable phase is a monolayer in some temperature range. In any other case, however, it remains controversial whether the graphite overlayer is really a monolayer or not. In the literature, LEED (Refs. 7 and 13) and surface-enhanced electron-energy-loss fine-structure spectroscopy[8,10] (SEELFS) studies show that the distances are fairly large between the monolayer graphite and the substrate metals. Moreover, a model was proposed based on experiments of alkali-metal adsorption on graphite-covered metals,[14,15] in which the graphite layer is understood to be raised up except at the edge region of the island. Consequently, the model provides that the interaction between monolayer graphite and a metal substrate is a van der Waals interaction and the bonding nature within the overlayer is unchanged.

On the other hand, in graphite intercalation compounds (GIC's), it is well known that the intercalant perturbs the electronic structure, lattice constant, and vibrational frequency of the host-graphite layer.[5] That is, the intercalant works as a donor or an acceptor, and gives or receives electrons from the graphite plane without significantly changing its electronic band structure. Such a scheme is called a "rigid-band model." Naturally, a similar process is expected between the monolayer graphite and the substrate, but there is little available information about the intralayer bond change of the monolayer graphite. Only its cohesion energy was discovered to be greater than that of the bulk graphite.[7]

Very recently we found anomalous softening of phonons in the monolayer graphite and a relatively large interaction between the overlayer and the substrate.[16] We present in this paper a detailed study of the phonon structure in monolayer graphite investigated by electron-energy-loss spectroscopy (EELS). The bond in the overlayer experiences a considerable softening effect from the substrate; this effect depends largely on the substrate structure just below the overlayer.

II. EXPERIMENT

The apparatus used in this investigation was a high-resolution EELS spectrometer equipped with a two-grid LEED system, a cylindrical mirror analyzer for AES, an ion-bombardment gun, and a gas-introduction system. The spectrometer consisted of a double-pass electrostatic cylindrical-deflector-type monochromator and analyzer,

which achieved an energy resolution of 4–6 meV at a sample current of 10^{-10} A. The optimum design of the spectrometer was described elsewhere.[17] The spectrometer chamber was magnetically triply shielded with alloys of high permeability, and was evacuated by a diffusion pump with a liquid-nitrogen-cooled trap and a titanium-sublimation pump. After 24 h of baking at temperatures up to 180 °C, the base pressure was less than 2×10^{-8} Pa.

The specimens used in this investigation as substrates were TaC(111), TaC(001), TiC(111), TiC(001), HfC(111), and HfC(001). They were cut from single-crystalline rods in disk shape pieces about 8 mm in diameter and 1 mm in thickness using the spark-erosion method. The single-crystalline rods were each grown in our laboratory by the zone-leveling floating-zone method.[18–21] One side of the disks was mechanically polished to a mirror finish with diamond paste, and ultrasonically cleaned with acetone. One of these prepared specimens was attached to the sample holder and was put into the vacuum. After baking, the specimen was cleaned by heating up to about 1700 °C in an ultrahigh vacuum (UHV). The sample temperature was measured by a two-color optical pyrometer. This procedure made each sample so clean that LEED showed a sharp low-background 1×1 pattern and no impurity was detected by AES. These transition-metal carbides have rock-salt structure. It has been revealed that the clean (001) surface is a "neutral" surface, in which metal and carbon atoms are arrayed alternately. On the other hand, the clean (111) surface is "polar" and consists of metal-atom termination.[22,23]

The graphitic overlayer was grown on this surface by exposure to ethylene gas while keeping the sample at high temperature. The necessary amount of the exposure depends on the substrate: The monolayer graphite was readily formed on the (111) surfaces at a relatively small exposure of a few hundred langmuirs (1 L $=1\times10^{-6}$ Torr sec). On the other hand, the (001) surfaces are less able to form a graphitic layer. On TaC(001), the necessary exposure was more than several thousand langmuirs, and on TiC(001) and HfC(001) the graphitic layer was not able to form at exposures up to 100 000 L in the temperature range of 800–1600 °C.

The EELS spectrum of the prepared graphite monolayer was measured along the $\bar{\Gamma}$–$\bar{M}$ direction of the overlayer. The detection polar angle θ_f was fixed at 72° and the incident angle θ_i was varied to obtain a wave vector parallel to the surface. The incident beam energy E_0 of 15–25 eV was used. The momentum transfer parallel to the surface $q_\parallel$ is given as

$$q_\parallel=\frac{\sqrt{2mE_0}}{\hbar}(\sin\theta_f-\sin\theta_i)\ , \tag{1}$$

which corresponds to the surface-phonon wave number as a result of the momentum-conservation law. In Eq. (1), m is electron mass and $\hbar$ is Planck's constant. Since the energy loss by the phonon excitation is much smaller than E_0, the energy difference between the primary and outgoing beams is neglected in Eq. (1). Typical measuring time for one spectrum was about 10 min under specular conditions, and 1–3 h under off-specular conditions. As the graphite is very inert, little trace of contamination from the residual gas was detected after a few days elapsed in a UHV.

III. RESULTS

A. Graphite on TaC(111)

When the clean TaC(111) was exposed to 200 L of ethylene at temperatures of 800–1200 °C, the LEED pattern changed from 1×1 into an incommensurate two-domain epitaxial pattern as shown in Fig. 1, and the AES spectrum changed from Fig. 2(a) to 2(b). The peak profile of the C *KVV* Auger signal at ~272 eV changes from "carbidic" in Fig. 2(a) to "graphitic" in 2(b).[24] In Fig. 1, $\mathbf{c}_1$ and $\mathbf{c}_2$ are the unit vectors of the substrate's reciprocal lattice, $\mathbf{g}_1,\mathbf{g}_2$ and $\mathbf{h}_1,\mathbf{h}_2$ are each unit vectors of the two-domain overlayers. The lattice constant a of the overlayer is estimated at 2.53±0.02 Å from the LEED patterns, regarding the substrate lattice constant as 3.15 Å. This value is 3±1% larger than the bulk graphite (a=2.46 Å). The azimuthal-epitaxial relationships are $\langle10\bar{1}0\rangle_C\|\langle1\bar{1}0\rangle_{TaC}$ for the domain of $\mathbf{g}_1$ and $\mathbf{g}_2$, and $\langle11\bar{2}0\rangle_C\|\langle1\bar{1}0\rangle_{TaC}$ for $\mathbf{h}_1$ and $\mathbf{h}_2$. When the temperature during the deposition was relatively low (~800 °C), the domain of $\mathbf{g}_1$ and $\mathbf{g}_2$ was predominant, although the high background in LEED shows the lower quality of the overlayer graphite. On the contrary, the other domain ($\mathbf{h}_1$ and $\mathbf{h}_2$) was stronger on the sample grown at higher temperature (~1200 °C). Other spots in Fig. 1 are located at the positions of sum vectors of the substrate's and the overlayer's reciprocal-lattice vectors. For example, spot *A* in Fig. 1 is arrived at by adding one overlayer vec-

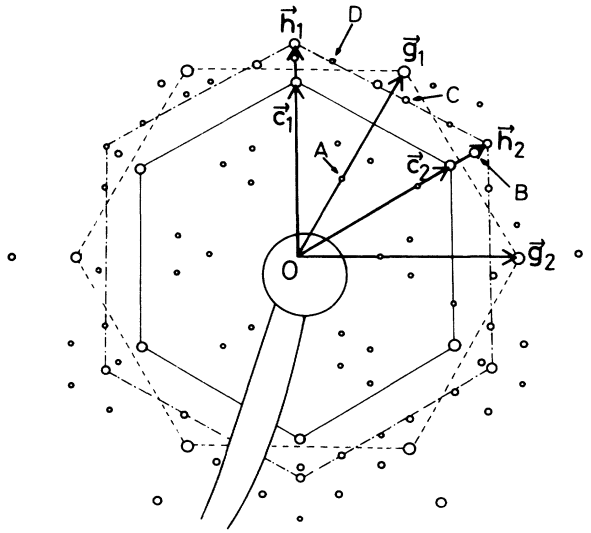

FIG. 1. Traced LEED pattern of the graphite-covered TaC(111). The primary energy was 150.2 eV. The hexagon connected by solid lines consists of fundamental spots of the substrate, and $\mathbf{c}_1$ and $\mathbf{c}_2$ are the reciprocal unit vectors. The dashed and dash-dotted lines indicate the two-domain overlayer graphite. $\mathbf{g}_1,\mathbf{g}_2$ and $\mathbf{h}_1,\mathbf{h}_2$ are their unit vectors. Any other spots such as *A*, *B*, *C*, and *D* are satellite spots, which are caused by the double diffraction as described in the text.

tor $(-\mathbf{g}_1)$ to one substrate fundamental $(\mathbf{c}_1+\mathbf{c}_2)$. Similarly B is $(\mathbf{g}_1+\mathbf{g}_2)+(-\mathbf{c}_2)$, C is $(-\mathbf{g}_1+\mathbf{g}_2)+(2\mathbf{c}_1)$, D is $(\mathbf{h}_2)+(\mathbf{c}_1-\mathbf{c}_2)$, and so on. These "satellite" spots are probably caused by the double diffraction. However, real structural or electronic modulation may be possible in the overlayer graphite. Independent of the modulation, the appearance of such satellites indicates that the overlayer graphite is so thin that the electron with an energy of ~150 eV can pass through it and reach the interface without inelastic scattering. Therefore the thickness of the overlayer should be comparable to or less than the mean free path of the electron beam of such an energy, which is about 10 Å at most.[25]

EELS measurement was performed on the sample grown at 1000 °C, which showed a typical two-domain structure. The azimuth was set to the $[1\bar{1}0]$ of the substrate. Figure 3(a) shows a specular EELS spectrum of this sample. At this primary energy and with this sample condition, no loss peak was observed clearly. However, when lower primary energy was used, several loss peaks sometimes appeared depending on the sample condition, as shown in Fig. 3(b). Above 200 meV, no loss peak was ever observed as long as the graphitic layer was clearly seen in LEED. This fact indicates perfect dissociation of C—H bonds. In the off-specular condition, fruitful loss features appeared. Figure 4 is a series of off-specular EELS spectra, in which five branches of loss peaks (LA,ZA,ZO,LO,R) can be seen clearly. Figure 5 shows the dispersion relation of these phonon modes. Each mode is assigned as follows: (1) The branch ZA is an

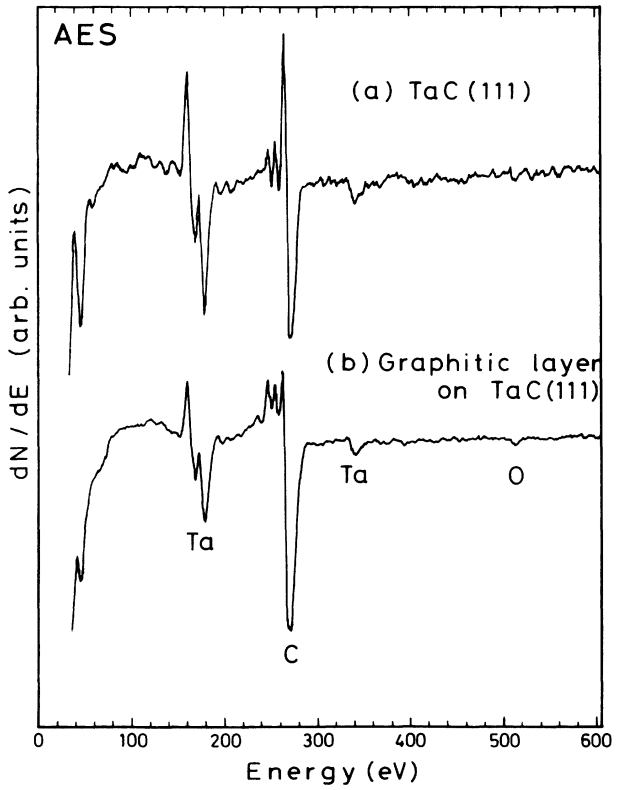

FIG. 2. AES spectra for (a) clean TaC(111) and (b) graphite-covered TaC(111).

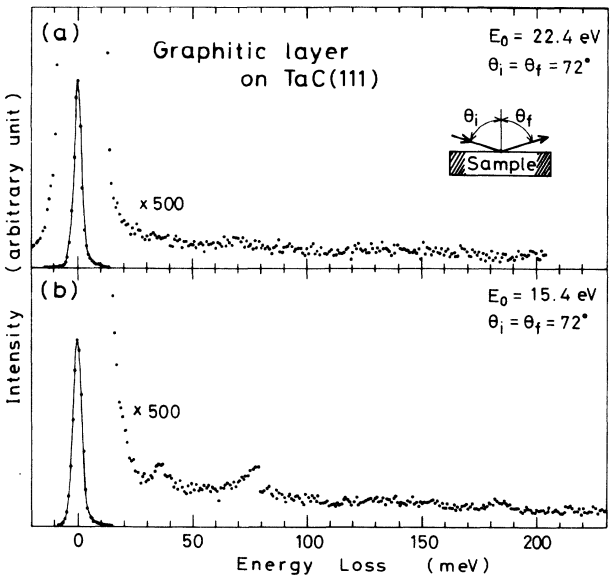

FIG. 3. Specular EELS for the graphite-covered TaC(111). (b) is a different run from (a). The primary beam energy is lower in (b), and three loss peaks appear at 34, 77, and 185 meV.

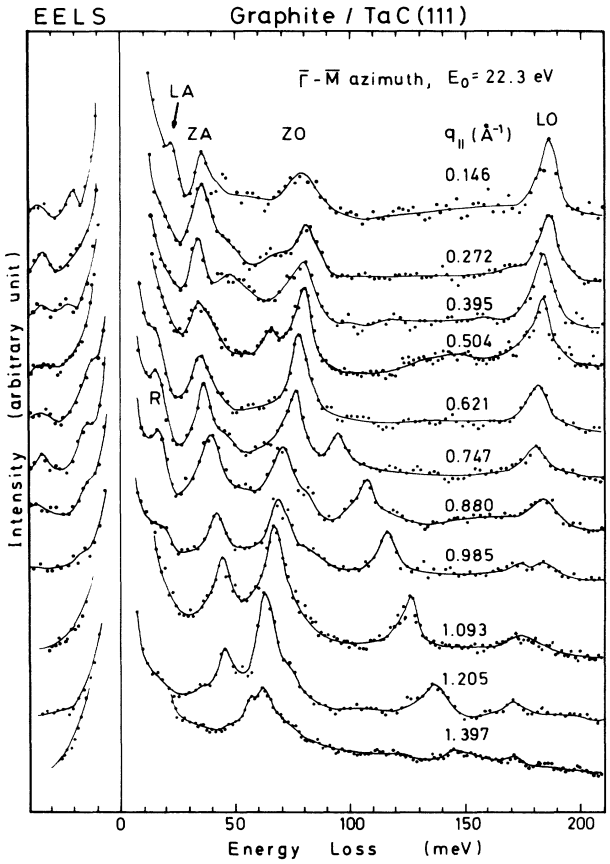

FIG. 4. Series of off-specular EELS for the graphite-covered TaC(111). Five loss peaks (LA, ZA, ZO, LO, and R) are assigned in the text. The curves are only intended to guide the eyes.

overlayer acousticlike mode in which the two carbon atoms in the unit mesh vibrate in phase and perpendicularly to the surface. (2) The branch ZO is a vertically vibrating optical mode of the overlayer. (3) The branch LA is a longitudinal-acoustic mode of the overlayer. As this branch changes little from the bulk graphite, we can easily identify the overlayer as graphite. (4) The branch LO is a longitudinal-optical mode of the overlayer. (5) The branch R is presumably a Rayleigh mode of the system including the substrate.

As the overlayer consisted of two domains, two sets of dispersion curves along $\bar{\Gamma}$-$\bar{M}$ and $\bar{\Gamma}$-$\bar{K}$ should be simultaneously detected. Because the dispersion relations along these two directions are almost the same in graphite, especially in the long-wavelength region, we were not able to discriminate these two clearly under the resolution of this experiment, even near the boundary of the surface Brillouin zone (SBZ).

Comparing the dispersion curves with the bulk one[26–28] shown in Fig. 6, some clear differences are realized: At first, the dispersion of the ZA mode is smaller in Fig. 5, and this branch has relatively high energy in the long-wavelength region compared with the bulk phonon band edge (the arrow BE in Fig. 6). This high frequency in the long-wavelength region indicates that the recovering force between the overlayer and the substrate is stronger than the van der Waals force. Secondly, the ZO mode is largely softened in Fig. 5. This softening and the small dispersion in the ZA mode indicate the large reduction of bending and twisting force constants within the overlayer. Thirdly, the branches LA and LO are also softened slightly. These changes will be discussed in Secs. IV and V. Finally, only four overlayer modes (ZA, ZO, LA, and LO) can be seen in Fig. 5, whereas two additional shear horizontal (SH) modes appear in Fig. 6. As the selection rule of EELS (Ref. 29) should forbid the SH modes to be detected in this experimental regime, this difference is ascribed to some peculiarity of the bulk graphite rather than the monolayer one, although it is not yet clear concretely what this peculiarity is.

When this surface was heated at a temperature higher than 1600 °C, the overlayer disappeared and the clean TaC(111) 1×1 surface was recovered easily, so that re-

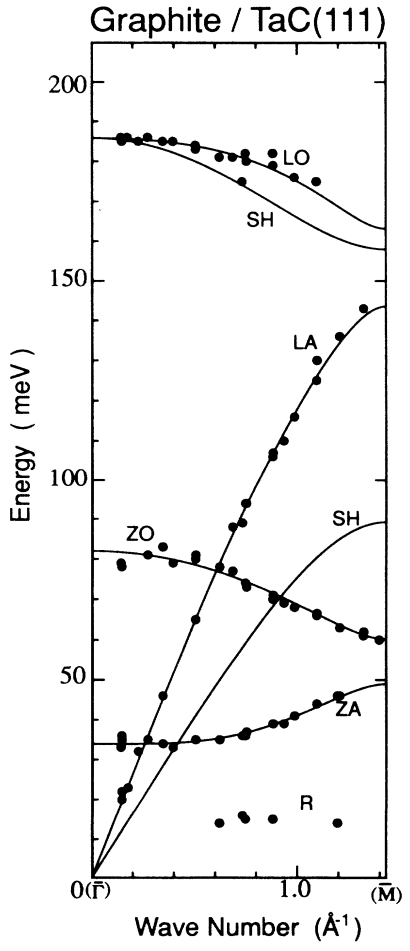

FIG. 5. Phonon-dispersion relations for the monolayer graphite on TaC(111). The results of the present experiment are indicated by dots, and lines are the result of the model calculation fitted to the data by using a least-squares method.

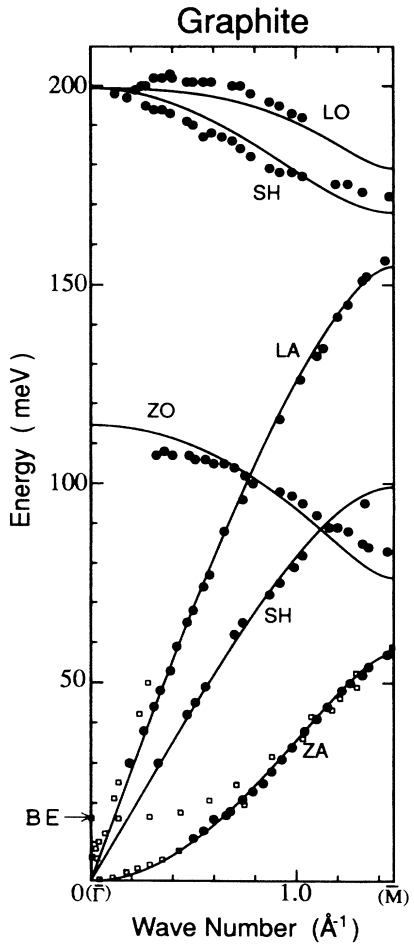

FIG. 6. Phonon dispersion for bulk graphite. Solid dots are the results of EELS (Ref. 26) and open squares are the result of inelastic neutron-scattering spectroscopy (Ref. 27). Lines are phonon-dispersion curves calculated by using a monolayer-graphite model to fit these experimental data.

peated experiments of deposition are possible. Even when the exposure to ethylene was increased to 1000 L, which is about one order of magnitude larger than the necessary amount, the results did not change in EELS or LEED. This fact indicates that the formation of the graphite spontaneously stops at finite thickness when the surface is saturated. Therefore the amount of the exposure is not critical for the overlayer thickness and the identical graphite-covered surface was easily reproducible. This thickness will be clarified to be a monolayer in Sec. V.

B. Graphite on HfC(111)

The procedure and the results are almost similar to TaC(111). The specimen exposed to 200 L of ethylene at 1050 °C showed a similar two-domain structure in LEED, and similar dispersion curves shown in Fig. 7. The quantity of the deviation from the bulk phonon is, however, a little different from that on TaC(111). The lattice constant is estimated to be 2.49±0.02 Å.

C. Graphite on TiC(111)

Figure 8 shows the LEED pattern of the graphite on TiC(111) which was grown at 1100 °C by exposure to 200

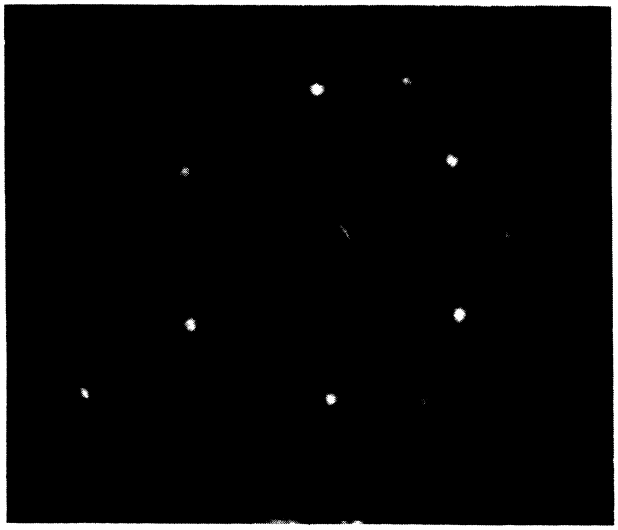

FIG. 8. LEED pattern for the graphite-covered TiC(111). Only one domain can be seen. Primary energy was 202.3 eV.

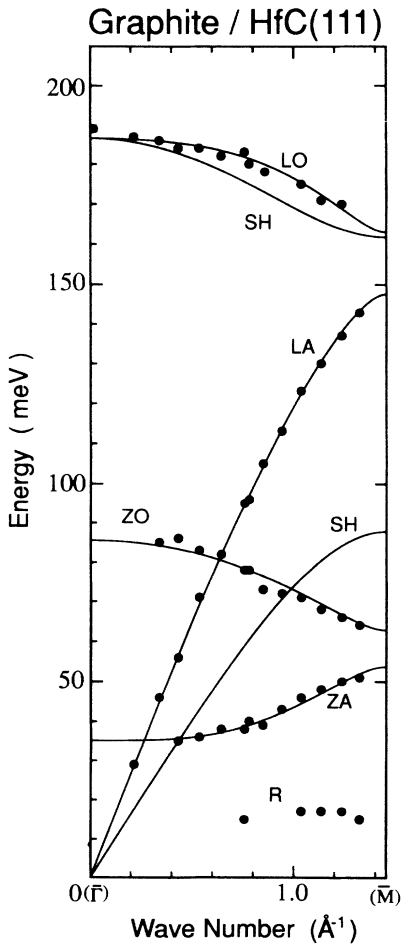

FIG. 7. Phonon-dispersion for the monolayer graphite on HfC(111).

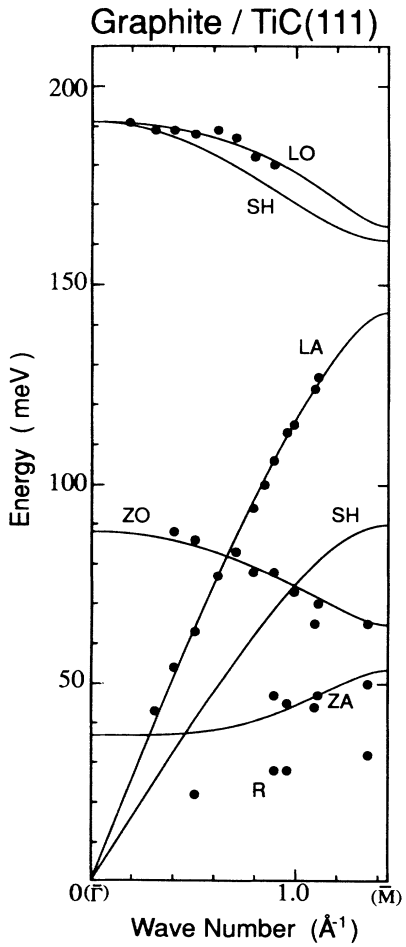

FIG. 9. Phonon dispersion for the monolayer graphite on TiC(111).

L of ethylene. In this case, only one domain $\langle 10\bar{1}0\rangle_C \| \langle 1\bar{1}0\rangle_{TiC}$ was observed with very low background, which shows the very good quality of the overlayer. TiC has a lower melting point than HfC or TaC, and therefore the bulk-crystal quality is better. Probably this higher crystal quality may cause the single-domain structure. The lattice constant of the overlayer is estimated at 2.50 ± 0.02 Å.

The phonon dispersion was measured along the $[1\bar{1}0]$ azimuth of the substrate which corresponds to the $\bar{\Gamma}$-$\bar{M}$ direction of the overlayer graphite. Figure 9 is the result. Since Ti is much lighter than Ta and Hf, the bulk acoustic-phonon band of the substrate covers a wide energy range up to 50 meV in the low-energy region.[30,31] Consequently, the low-energy branch of the overlayer, the ZA mode, becomes a resonance mode, and the vibrational amplitude decreases in the overlayer. This is the reason why the ZA mode has disappeared in the first half of the SBZ.

D. Graphite on TaC(001)

On TaC(001), the growing efficiency is much lower, and more than a few-thousand langmuirs of ethylene exposure is necessary to get a graphite-covered surface. Figure 10 shows the LEED pattern of the sample exposed at 1500 °C to ethylene of 50 000 L. Double-diffraction spots can be seen also in Fig. 10, which indicates the thinness of the overlayer graphite. When the temperature during the deposition was lower (800–1200 °C), a ring pattern appeared in the LEED, which means random orientation of the graphite overlayer around the c axis. In contrast, at higher temperature ($\sim$1500 °C), only the two-domain epitaxial structure was formed as shown in Fig. 10. The epitaxial relationships are $(0001)_C \| (001)_{TaC}$ and $\langle 11\bar{2}0\rangle_C \| \langle 110\rangle_{TaC}$. As TaC[110] is equivalent to TaC[$1\bar{1}0$], the domain of $\langle 11\bar{2}0\rangle_C \| \langle 1\bar{1}0\rangle_{TaC}$, or $\langle 10\bar{1}0\rangle_C \| \langle 110\rangle_{TaC}$, also exists. The resultant two-domain LEED pattern seems at first sight like a centered

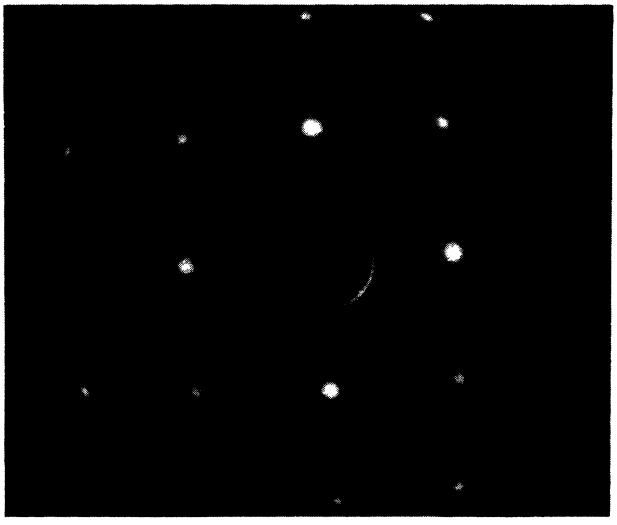

FIG. 10. LEED pattern for the graphite-covered TaC(001). $E_0 = 227.1$ eV.

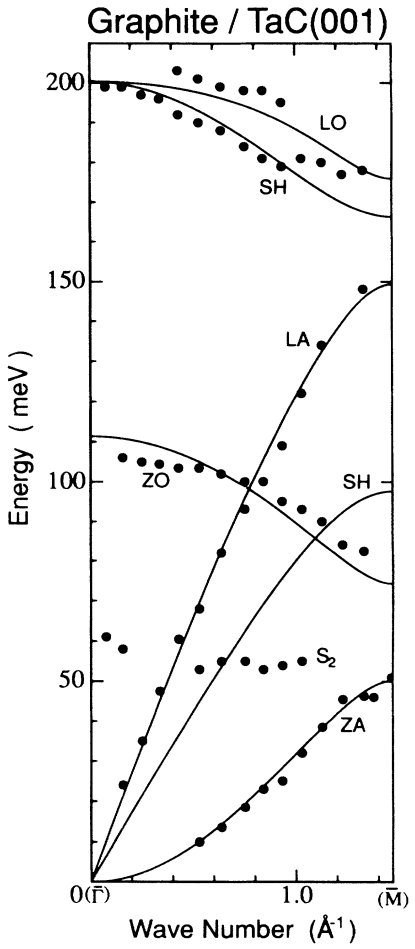

FIG. 11. Phonon dispersion for the graphite overlayer on TaC(001).

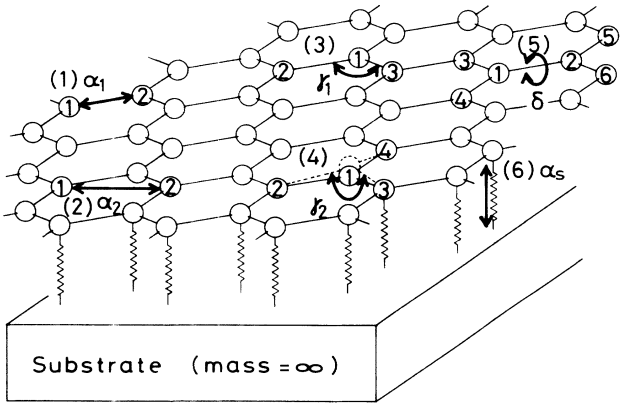

FIG. 12. Illustration for the force-constant parameters. α_1 and α_2 are stretching force constants. γ_1 is an in-plane and γ_2 is an out-of-plane bond-bending force constant. δ is a twisting force constant and α_s represents the interaction between the overlayer and the substrate.

4×4 pattern, but the detailed observation clarified that this pattern is not exactly c-4×4, so that we might call this "pseudo-c-4×4." The estimated lattice constant from the LEED pictures is 2.46±0.02 Å, which is just the same as pristine graphite.

Figure 11 shows the phonon-dispersion curves of this system. In contrast with the case on the (111) surfaces, the measured phonon dispersion is very similar to the bulk one (Fig. 6). The ZA and the ZO modes do not change as much as graphite on TaC(111) (Fig. 5). The differences between Figs. 11 and 6 are as follows: (1) The acoustic SH mode does not appear in Fig. 11. (2) The mode of small dispersion appears in Fig. 11 at the energy of 50–60 meV, which is assigned to be the S_2 mode (Wallis mode) of the substrate.[32,33] It is not clear whether this mode came from the substrate "under" the overlayer graphite, or the overlayer deposition was not perfect and the remaining bare substrate contributed to the data. (3) The ZA mode is softened in Fig. 11 at the boundary region of the SBZ, although the difference is small.

IV. DYNAMICAL MODEL CALCULATION

To analyze the phonon-dispersion data, the dispersion relation of the monolayer graphite was calculated by using the force-constant model presented hereafter, and was fitted to the experimental data. Six phenomenological force-constant (FC) parameters were adopted in this model. The definitions of each FC in a potential term of the model Hamiltonian are given in the Appendix. Figure 12 schematically shows the following parameters: (1) α_1 is a stretching FC between the nearest neighbors, and (2) α_2, between the second-nearest neighbors. (3) γ_1 represents a three-body in-plane angle-bending FC. (4) γ_2 represents a four-body out-of-plane angle-bending FC, which causes the recovering force to keep flat the three nearest-neighbor bonds of one atom [atom 1 in part (4) of Fig. 12]. If this atom deviates upward, leaving the three nearest-neighbor atoms at the mean position, as shown by the dashed line in Fig. 12, this force works to return them to the same plane. (5) δ is a twisting FC, which represents a force similar to that keeping the ethylene molecule flat. (6) α_s is a stretching FC between the overlayer and the substrate.

In this model, the substrate is assumed to be rigid, structureless, and infinitely massive. Parallel components to the surface are not taken into account for the interaction between the overlayer and the substrate, because the structure is incommensurate and such components are though to be very small. The assumption that the substrate has infinite mass is appropriate for TaC and HfC. In these materials, the bulk phonon band splits into two relatively narrow bands because of the contrast between the metal's heaviness and the carbon's lightness. One is the acoustic band below 30 meV, and the other is the optical one located in the range 65–80 meV.[34] Since almost all of the overlayer phonon modes appear in the region unoccupied by the bulk band, the vibration of the overlayer does not penetrate into the bulk. Consequently, the vibrational amplitude of the overlayer mode is sharply localized at the overlayer. Although the ZO mode on C/TaC(111) and C/HfC(111) appears at the optical-band region, the interaction between the bulk phonon and the overlayer should be small on the (11$\bar{1}$) surface, because, in the optical branch, the amplitude is mainly distributed to carbon in the substrate, and the outermost metal vibrates little. On TaC(001), the ZO mode appears above the optical band and no interaction is expected. For TiC, on the contrary, this heavy-substrate approximation is not suitable, and in fact, the ZA mode disappears in the first half of the SBZ probably because of the large interaction between this mode and the substrate acoustic phonon, which spreads up to ~50 meV in this matter. However, it is very difficult to take into account the substrate structure because the overlayer is incommensurate with the substrate. Therefore, we reluctantly adopted the same model for the graphite on TiC(111), too.

The dispersion curves were calculated in accordance with the ordinary harmonic method; at first the force-constant matrix was calculated from the model Hamiltonian, then the dynamical matrix corresponding to a given wave vector was calculated and diagonalized. The square root of the resultant eigenvalue is the frequency of

TABLE I. Force constants and their deviations from pristine graphite.

Force constants	Pristine graphite	Graphite on TaC(111)	Graphite on HfC(111)	Graphite on TiC(111)	Graphite on TaC(001)
a (Å)	2.46	2.53±0.02	2.49±0.02	2.50±0.02	2.46±0.02
Δa (%)		+3±1	+1±1	+2±1	0±1
α_1 (10^5 dyn/cm)	7.28	6.56	6.92	6.92	7.25
$\Delta\alpha_1$ (%)		−10	−5	−5	±0
α_2 (10^5 dyn/cm)	1.24	0.98	1.04	0.85	1.01
$\Delta\alpha_2$ (%)		−21	−16	−32	−19
γ_1 (10^{-12} erg)	8.30	7.18	6.49	7.49	8.53
$\Delta\gamma_1$ (%)		−13	−22	−10	+3
γ_2 (10^{-12} erg)	3.38	1.52	1.61	1.71	3.21
$\Delta\gamma_2$ (%)		−55	−52	−50	−5
δ (10^{-12} erg)	3.17	1.16	1.74	1.44	1.98
$\Delta\delta$ (%)		−64	−45	−55	−38
α_s (10^4 dyn/cm)		5.30	5.69	6.24	0

the phonon.

In the previous Letter,[16] we fitted the calculated dispersion curve to the experimental data by adjusting the phonon frequency calculated at the highly symmetric point to the experimental value. If such calculated dispersion curves gave a poor agreement with the experimental data as a whole, the parameters were changed gradually until they fitted best, judging by the eye. In this paper, on the other hand, we adopted a least-squares method to improve the reliability. Therefore the estimated FC values listed in Table I have a little difference from those in the previous Letter, although the essential features are the same.

The solid curves in Figs. 5, 6, 7, 9, and 11 are the fitted calculation results. In the values in Table I, α_s, γ_2, and δ in the C/TiC(111) case and α_2 in every sample have ambiguity. To estimate α_s, the most important data are the phonon frequencies of the ZA mode near the $\bar{\Gamma}$ point which have not been observed in the TiC case. Moreover, the adopted model is inadequate for the graphite on TiC(111) as mentioned above, and therefore the reliability of the estimated parameter set for this system is low. As for α_2 values, the absolute quantity of this value is by nature much smaller than α_1, and small deviation of this value hardly affects the result. The other parameters are expected to have much higher reliability.

V. DISCUSSION

As shown in Table I, the FC's related to the vertical vibration, γ_2 and δ, are much softer than those for the horizontal vibration, α_1 and γ_1, on the (111) surfaces. The softening in the former reach as much as 60%, while the latter is restricted within 20%. This difference and the origin of the softening are discussed in this section.

In graphite, the sp_2-hybridized orbital forms a σ bond which principally makes the honeycomb structure of graphite. The remaining p_z electron is distributed on both sides of the honeycomb plane and forms a π bond. The electronic structure of the one-atomic-layer graphite has been calculated theoretically, and it has been revealed that the σ band has the character of a covalent bond with a large band gap; on the other hand, the π band composes a zero-gap semiconductor structure.[35] From the viewpoint of the arrangement of each bond in real space, the π bond must affect γ_2 and δ more than α_1 or γ_1. When the basal plane is bent, the overlap of the π orbital is changed more than the σ orbital. On the contrary, by the deformation parallel to the plane, the σ orbital is directly affected as well as the π bond. Consequently, the large difference in softening between (γ_2,δ) and (α_1,γ_1) can be explained by the different reduction of the π bond from the σ bond. If the π bond becomes much weaker than the σ bond, the FC's γ_2 and δ on which the π bond directly works must be very softened, whereas γ_1 and α_1 will not be so affected because the contribution of the σ bond is larger. This situation, that the π bond becomes much softer than the σ bond, is very probable from an electronic point of view, because it is the π band that is near the Fermi level.

It has been clarified by ultraviolet photoemission spectroscopy (UPS) experiments that the monolayer graphite on Ni(111),[9] Ni(110),[11] and Ni(001)[12] has a very similar electronic structure to pristine graphite except for the overall shift of the band toward higher binding energy. A similar shift has been observed in the alkali-metal GIC's (Ref. 36) and it is ascribed to an increase in the Fermi level caused by the charge transfer from the intercalant to the host-graphite layer. In analogy with this, the band shift in the monolayer graphite on Ni has been interpreted as being caused by the charge transfer from the substrate Ni to the overlayer graphite. When an electron flows into the graphite, it inevitably occupies the antibonding π band. Therefore such charge transfer should soften the π bond more, consistently with the model mentioned above.

Ab initio theoretical calculation[37,38] revealed that the electron transfer into the graphitic plane causes the expansion of the lattice and the softening of the parallel vibration mode at the $\bar{\Gamma}$ point. However, it is not strictly clear how the phenomenological FC adopted here changes with the charge transfer, even though our model described above seems very probable. We look forward to more theoretical work. Nevertheless, it should be remarked that the amount of the deviation of each parameter from pristine graphite is very large in the monolayer graphite compared with the GIC case. For example, the lattice constant a of LiC_6 is increased by 1% compared with pristine graphite, while the deviation is as large as 2–3 % in the monolayer graphite.

As for the thickness of the overlayer graphite, we now get very reliable information indicating "monolayer." At first, the electron beam used here in EELS can "see" or penetrate up to the interface between the overlayer and the substrate, because its mean free pass is larger than that used in LEED and even the electron beam in LEED can pass through the overlayer as indicated by the satellite spots. Secondly, only one set of phonons appeared in EELS and they were very much modified. As known in GIC's,[5,38,39] the effect of charge transfer is restricted to the boundary layer (the layer directly attached to the intercalant) and the interior layer is affected only by the secondary lattice expansion or contraction effect. In fact, the two phonons were observed in the Raman and infrared spectrum from alkali-metal GIC's;[5,40] one of them comes from the boundary layer and is more affected, while the other from the interior layer slightly changes its frequency. Similarly, if the overlayer consisted of more than two layers, the phonon structure in the layer connected directly to the substrate should be different from the others and at least two separate phonon sets should be observed in EELS. However, all the measurements in this experiment showed only one set of phonon-dispersion curves to indicate just the monolayer.

The graphite layer on TaC(001) is a special case, in which the phonon softening hardly occurs. In this case, we cannot affirm from our logic that the overlayer is the monolayer, but it is certain that the layer attached directly to the substrate shows little change in its dynamical properties from bulk graphite, because the LEED also showed the satellites and the EELS also indicated one set of phonons. In this case, therefore, the charge transfer

ought not to occur. Perhaps this lack of the charge transfer causes very small interaction α_s between the overlayer and the substrate, and because of this small α_s we can observe the ZA mode even within the bulk acoustic band. On the contrary, the large charge transfer from the substrate to the monolayer graphite might produce the relatively strong α_s interaction as in the case of monolayer graphite on the (111) surfaces. The contrast between C/TaC(111) and C/TaC(001) shows that it is not the macroscopic properties of the substrate but the microscopic structure in the vicinity of the interface that determines the degree of the charge transfer.

VI. CONCLUSIONS

The graphite formation on (001) and (111) surfaces of some transition-metal carbides was investigated and it was revealed that the monolayer graphite is easily formed on the (111) surfaces of TaC, HfC, and TiC, and not so readily on TaC(001) nor on HfC(001) nor on TiC(001). The phonon-dispersion relation of the overlayer was measured by EELS, and the monolayer graphite on the (111) surfaces was clarified to have a very different phonon structure from pristine graphite. In contrast with this, the graphite on TaC(001) is hardly affected. The phonon structures were analyzed with a force-constant model, and it was revealed that the force constants related to vertical motion in the monolayer graphite are very much softened. This softening is presumably caused by the selective softening of the π bond. This model of π bond softening is consistent with the charge transfer from the substrate into the overlayer. The contrast between C/TaC(111) and C/TaC(001) shows that the microscopic atomic structure at the interface is important to the charge transfer.

ACKNOWLEDGMENTS

We acknowledge Professor S. Tanuma, Professor K. Nakao, and Professor H. Suematsu for stimulating discussions.

APPENDIX

In the dynamical model adopted here, the potential term of the model Hamiltonian is defined by using each force-constant parameter as follows.

(1) The potential energy between atoms 1 and 2 in Fig. 12, parts (1) or (2) is

$$\frac{\alpha}{2}\left[\frac{(\mathbf{u}_2-\mathbf{u}_1)\cdot\mathbf{r}_{12}}{|\mathbf{r}_{12}|}\right]^2,$$

where $\mathbf{u}_i$ indicates the displacement vector of the atom i, and $\mathbf{r}_{ij}$ the relative mean position of the atom j from the atom i. α represents α_1 in the case when atoms 1 and 2 are nearest neighbors, and α_2 in the case when they are second-nearest neighbors.

(2) The potential energy corresponding to the in-plane angle bending as shown in Fig. 12, part (3) is

$$\frac{\gamma_1}{2}\left[\left[\frac{(\mathbf{u}_2-\mathbf{u}_1)\times\mathbf{r}_{12}}{|\mathbf{r}_{12}|^2}\right]_z-\left[\frac{(\mathbf{u}_3-\mathbf{u}_1)\times\mathbf{r}_{13}}{|\mathbf{r}_{13}|^2}\right]_z\right]^2.$$

The subscript z means the component perpendicular to the surface.

(3) In the case of graphite, carbon composes the sp_2-hybridized orbital, the length of the three nearest-neighbor bonds are the same, and the triangle formed by the three nearest-neighbor atoms [atoms 2,3,4 in Fig. 12, part (4)] of one atom (atom 1) is regular. So the term for the out-of-plane angle bending becomes very simple as follows:

$$\frac{\gamma_2}{2}\left[\frac{u_{2z}+u_{3z}+u_{4z}-3u_{1z}}{|\mathbf{r}|}\right]^2,$$

where $|\mathbf{r}|\equiv|\mathbf{r}_{12}|=|\mathbf{r}_{13}|=|\mathbf{r}_{14}|=a/\sqrt{3}$.

(4) The twisting potential energy between atoms 1 and 2 in Fig. 12, part (5), is

$$\frac{\delta}{2}\left[\frac{(u_{5z}-u_{6z})-(u_{3z}-u_{4z})}{a}\right]^2.$$

(5) The potential energy between the overlayer and the substrate is assumed to be

$$\frac{\alpha_s}{2}u_z^2.$$

In this model, the dynamical matrix can be separated into two parts; one is the horizontal vibration and the other is the vertical. The former part includes the parameters α_1, α_2, and γ_1, and defines the dispersion of LA, LO, and SH modes. On the other hand, the latter includes γ_2, δ, and α_s, and defines ZA and ZO modes. The phonon frequency at the highly symmetric points are

$$\omega(\mathrm{LA},\bar{M})=[(3\alpha_2+\alpha_1)/m]^{1/2},$$

$$\omega(\mathrm{LO},\bar{\Gamma})=[(54\gamma_1/a^2+3\alpha_1/2)/m]^{1/2},$$

$$\omega(\mathrm{LO},\bar{M})=[(54\gamma_1/a^2+3\alpha_2+\alpha_1/2)/m]^{1/2},$$

$$\omega(\mathrm{ZA},\bar{\Gamma})=(\alpha_s/m)^{1/2},$$

$$\omega(\mathrm{ZA},\bar{M})=[(12\gamma_2/a^2+16\delta/a^2+\alpha_s)/m]^{1/2},$$

$$\omega(\mathrm{ZO},\bar{\Gamma})=[(108\gamma_2/a^2+\alpha_s)/m]^{1/2},$$

$$\omega(\mathrm{ZO},\bar{M})=[(48\gamma_2/a^2+\alpha_s)/m]^{1/2}.$$

In these expressions, m denotes the mass of a carbon atom.

To fit the calculated dispersion to the measured one, the parameters were determined by using a least-squares method. In the fitting procedure, we assumed the parameter α_s to be zero in the pristine graphite and the graphite on TaC(001), because the ZA branch seems to start from the origin at the $\bar{\Gamma}$ point in these cases. In fact, when this parameter was set free, this procedure seldom gave a minus value which is physically meaningless.

In the case of bulk graphite, it has been revealed that the "surface modes," in which the vibrational amplitude is large at surface layers, are located energetically just below the corresponding bulk phonon band.[41] In the

EELS experiment those surface modes should be observed, and therefore the ZA branch is settled into the origin at the $\bar{\Gamma}$ point. But this does not at all mean the nonexistence of the interlayer interaction. This inconsistency is produced by applying the monolayer model to the bulk surface phonon. In the case of C/TaC(001), on the contrary, the interaction between the graphite layer and the substrate is possibly very weak. If the overlayer composes a multilayer, the adopted model is not the case, so we cannot say anything about the amount of α_s. But if the monolayer is the case, the interaction α_s should be very small.

[1]C. A. Selloni, P. Carnevali, G. D. Chen, and E. Tosatti, Phys. Rev. B **31**, 2602 (1985).

[2]G. Binnig, H. Fuchs, Ch. Gerber, H. Rohrer, E. Stoll, and E. Tosatti, Europhys. Lett. **1**, 31 (1986).

[3]G. Binnig, Ch. Gerber, E. Stoll, T. R. Alberecht, and C. F. Quate, Europhys. Lett. **3**, 1281 (1987).

[4]For example, K. J. Strandburg, Rev. Mod. Phys. **60**, 161 (1988).

[5]M. S. Dresselhaus and G. Dresselhaus, Adv. Phys. **30**, 139 (1981).

[6]S. A. Solin and H. Zabel, Adv. Phys. **37**, 87 (1988).

[7]M. Eizenberg and J. M. Blakely, Surf. Sci. **82**, 228 (1979).

[8]R. Rosei, M. De Crescenzi, F. Sette, C. Quaresima, A. Savoia, and P. Perfetti, Phys. Rev. B **28**, 1161 (1983).

[9]R. Rosei, S. Modesti, F. Sette, C. Quaresima, A. Savoia, and P. Perfetti, Phys. Rev. B **29**, 3416 (1984).

[10]L. Papagno and L. S. Caputi, Phys. Rev. B **29**, 1483 (1984).

[11]L. Papagno, M. Conti, L. S. Capti, J. Anderson, and G. J. Lapeyre, Surf. Sci. **219**, L565 (1989).

[12]C. F. McConville, D. P. Woodruff, and S. D. Kevan, Surf. Sci. **171**, L447 (1986).

[13]Hu Zi-pu, D. F. Ogletree, M. A. Van Hove, and G. A. Somorjai, Surf. Sci. **180**, 433 (1987).

[14]N. R. Gall', S. N. Mikhaylov, E. V. Rut'kov, and A. Ya. Tontegode, Fiz. Tverd. Tela (Leningrad) **27**, 2351 (1985) [Sov. Phys.—Solid State **27**, 1410 (1985)].

[15]N. A. Kholin, E. V. Rut'kov, and A. Y. Tontegode, Surf. Sci. **139**, 155 (1984).

[16]T. Aizawa, R. Souda, S. Otani, Y. Ishizawa, and C. Oshima, Phys. Rev. Lett. **64**, 768 (1990).

[17]C. Oshima, R. Souda, M. Aono, and Y. Ishizawa, Rev. Sci. Instrum. **56**, 227 (1985).

[18]S. Otani, T. Tanaka, and Y. Ishizawa, J. Cryst. Growth **55**, 431 (1981).

[19]S. Otani and T. Tanaka, J. Cryst. Growth **51**, 381 (1981).

[20]S. Otani, S. Honma, T. Tanaka, and Y. Ishizawa, J. Cryst. Growth **61**, 1 (1983).

[21]S. Otani, T. Tanaka, and Y. Ishizawa, J. Cryst. Growth **97**, 522 (1989).

[22]M. Aono, Nucl. Instrum. Methods Phys. Res. B **2**, 374 (1984).

[23]R. Souda, T. Aizawa, S. Otani, and Y. Ishizawa, Surf. Sci. **232**, 219 (1990).

[24]J. T. Grant and T. W. Haas, Surf. Sci. **24**, 332 (1971).

[25]Data for diamond exist; B. B. Pate, Surf. Sci. **165**, 83 (1986).

[26]C. Oshima, T. Aizawa, R. Souda, Y. Ishizawa, and Y. Sumiyoshi, Solid State Commun. **65**, 1601 (1988).

[27]R. Nicklow, N. Wakabayashi, and H. G. Smith, Phys. Rev. B **5**, 4951 (1972).

[28]J. L. Wilkes, R. E. Palmer, and R. F. Willis, J. Electron Spectrosc. Relat. Phenom. **44**, 355 (1987).

[29]H. Ibach and D. L. Mills, *Electron Energy Loss Spectroscopy and Surface Vibrations* (Academic, New York, 1982), p. 116.

[30]C. Oshima, T. Aizawa, M. Wuttig, R. Souda, S. Otani, Y. Ishizawa, H. Ishida, and K. Terakura, Phys. Rev. B **36**, 7510 (1987).

[31]H. Ishida and K. Terakura, Phys. Rev. B **36**, 4403 (1987).

[32]C. Oshima, R. Souda, M. Aono, S. Otani, and Y. Ishizawa, Solid State Commun. **57**, 283 (1986).

[33]H. Ishida and K. Terakura, Phys. Rev. B **34**, 5719 (1986).

[34]H. Bitz and W. Kress, *Phonon Dispersion Relations in Insulators* (Springer-Verlag, New York, 1979), pp. 65 and 70.

[35]G. S. Painter and D. E. Ellis, Phys. Rev. B **1**, 4747 (1970).

[36]G. K. Wertheim, P. M. Th. M. Van Attekam, and S. Basu, Solid State Commun. **33**, 1127 (1980).

[37]C. T. Chan, W. A. Kamitakahara, K. M. Ho, and P. C. Eklund, Phys. Rev. Lett. **58**, 1528 (1987).

[38]C. T. Chan, K. M. Ho, and W. A. Kamitakahara, Phys. Rev. B **36**, 3499 (1987).

[39]C. T. Chan, W. A. Kamitakahara, and K. M. Ho, Synth. Metals **23**, 327 (1988).

[40]S. Y. Leung, G. Dresselhaus, and M. S. Dresselhaus, Synth. Metals **2**, 89 (1980).

[41]E. de Rouffignac, G. P. Alldredge, and F. W. de Wette, Phys. Rev. B **23**, 4208 (1981).

FIG. 10. LEED pattern for the graphite-covered TaC(001). $E_0 = 227.1$ eV.

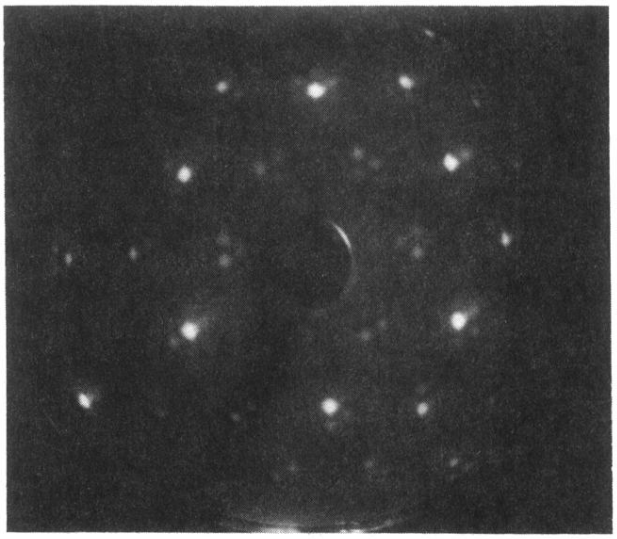

FIG. 8. LEED pattern for the graphite-covered TiC(111). Only one domain can be seen. Primary energy was 202.3 eV.